

USGS AWARD NUMBER 04HQGR0050

Principal Investigator: Gene Ichinose

Ground motion studies of modern and historical Cascadia intraslab earthquakes using one and three-dimensional waveform modeling methods to generate ground shaking maps

PROGRAM ELEMENT II

"Research supported by the U.S. Geological Survey (USGS), Department of the Interior, under USGS award number (04HQGR0050). The views and conclusions contained in this document are those of the authors and should not be interpreted as necessarily representing the official policies, either expressed or implied, of the U.S. Government."

Ground motion studies of modern and historical Cascadia intraslab earthquakes using one and three-dimensional waveform modeling methods to generate ground shaking maps

USGS AWARD #04HQGR0050
Final Technical Report

Gene A. Ichinose, Hong Kie Thio, Paul G. Somerville
URS Group, Inc., 566 El Dorado Street, 2nd Floor, Pasadena, CA 91101-2560
Phone 626-449-7650, Fax 626-449-3536, email gene_ichinose@urscorp.com

Abstract

We reanalyzed the April 13, 1949 Olympia, Washington earthquake using digitized records and first motion polarities from long-period seismograms. The moment tensor mechanism is normal faulting with a down dip trending T-axis similar in style to other Cascadia intraslab earthquakes. The total seismic moment is 1.3×10^{26} dyne-cm (M_w 6.7) and the hypocenter depth is 60 km. Additional inverse modeling for the kinematic rupture process assuming the steeply east dipping fault plane from the moment tensor resulted in a slightly higher total moment of 1.9×10^{26} dyne-cm (M_w 6.8). The earthquake ruptured to the south with at least 2 subevents.

The combined area of asperities and seismic moment for the 1949 earthquake were compiled with those from 1965 Seattle-Tacoma, 2001 Nisqually and those from Japan and Mexico to develop a source scaling relation separate from shallow global strike-slip earthquakes. We infer that deeper intraslab earthquakes have significantly smaller combined area of asperities than those compiled for shallower strike-slip earthquakes with the same seismic moment. This difference in rupture area leads to a 3 to 5 fold increase in stress drop for earthquakes with seismic moments between 10^{24} and 10^{28} dyne-cm.

1. Introduction

Intraslab earthquakes occur in the upper portion of the subducting Juan de Fuca Plate within the Cascadia Subduction zone beneath the Puget Sound region of western Washington. The largest were the 1949 Olympia (M 6.9-7.1), 1965 Seattle-Tacoma (M 6.8), and 2001 Nisqually (M 6.8) earthquakes (**Figure 1**). The hazards they pose are nearly equal to that from other seismic sources for time scales relevant to retrofitting (i.e., 50% Probability of exceedence in 75 years). The February 28, 2001 Nisqually earthquake caused over a billion dollars in losses. While retrofitting limited damages, continued efforts are needed because an earthquake closer to Seattle or larger in magnitude will cause more damage and disruption. Reexamination of historical earthquakes improves strong-ground motion prediction more than completely stochastic scenarios. This also better resolves how stresses are released in the subducting slab relative to tectonic forces and dehydration embrittlement (e.g., Kirby et al., 1995; Dobson et al., 2002) particularly since aftershocks from deep intraslab earthquakes are rare in the Pacific Northwest.

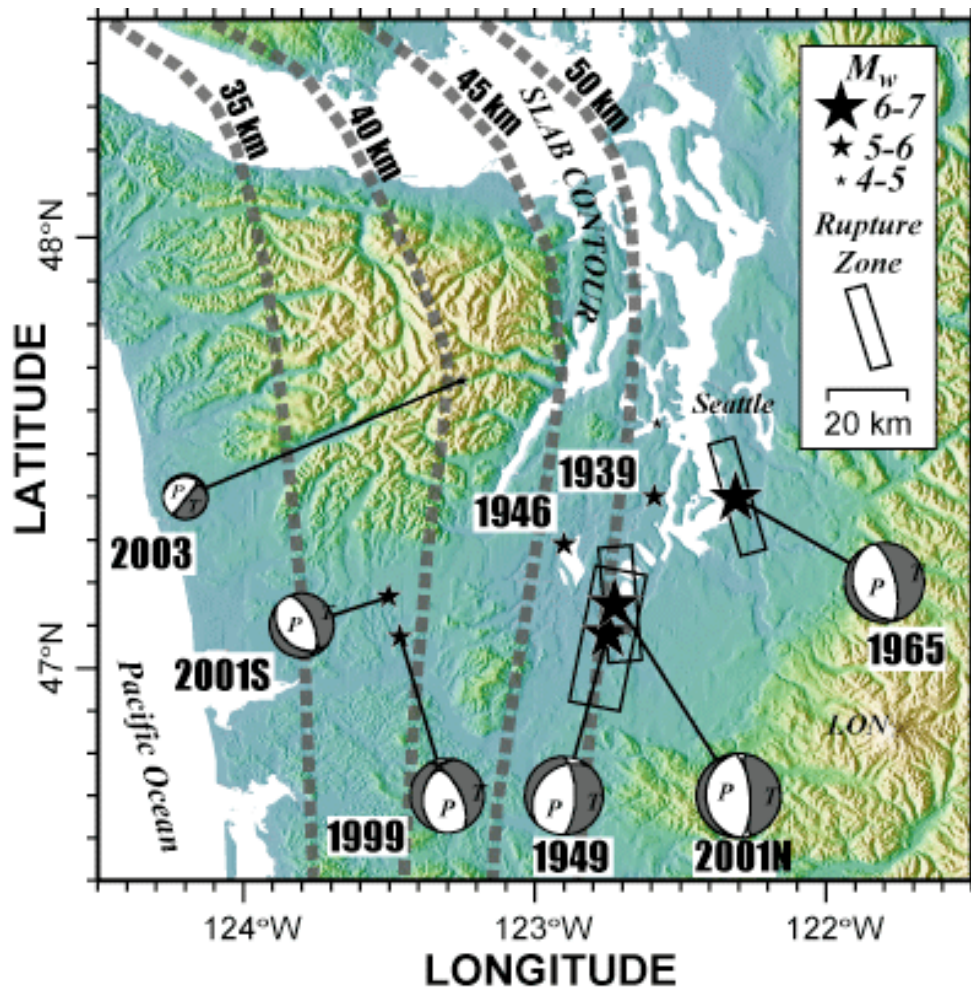


Figure 1. Locations and mechanisms of historical and modern Puget Sound intraslab earthquakes. The contours show the approximate depth to the top of the subducting Juan de Fuca plate. The depths of these earthquakes are located within 0-10 km below the top of this surface.

Figure 2 illustrates the differences in estimated focal mechanisms for the April 13, 1949 Olympia, Washington earthquake. Nuttli (1950) initially estimated an oblique normal-strike-slip mechanism with a WSW trending T-axis. Hodgson and Story (1954) later included additional first motions and estimated a thrust type mechanism. Barker and Langston (1987) examined 3-component waveform data and recognized reversed polarities for some of the data previously analyzed. They estimated a sinistral strike-slip mechanism for the 1949 earthquake with rupture along an east-west trending fault that contrasts with the normal faulting mechanisms and down dip trending T-axes of other Puget Sound intraslab earthquakes. An intraslab strike-slip mechanism is possible for Cascadia similar to those in the Nankai trough in Japan, because oblique subduction can reactivate preexisting fracture zones in the Juan de Fuca plate.

With the new global broadband data collected from the Nisqually earthquake, it was appropriate to reexamine all historical Puget Sound intraslab earthquakes using the recent earthquake as a reference event. We reanalyzed 1949 Olympia earthquake from the inversion of digitized seismograms collected by Barker and Langston (1987), Wiest et al. (2004), and additional long-period WWSSN data from College, Alaska, Bogota Columbia, and Pasadena, California for the moment tensor and kinematic rupture process. Ichinose et al. (2004) performed a similar analysis for the 1965 and 2001 intraslab earthquakes. The source parameters from these analyses and other global intraslab earthquakes are compiled and we provide a new source scaling relation between combined area of asperities and seismic moment that is significantly different from shallow crustal earthquakes.

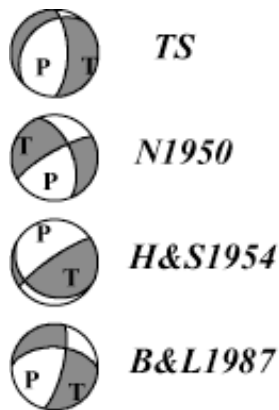


Figure 2. Focal mechanisms for the 13 April 1949 Olympia, Washington earthquake estimated by TS-this study using first motions and moment tensor inversion of teleseismic P-waves, N1950-Nuttli (1950) and H&S1954-Hodgson and Story (1954) using first motions, and B&L1987-Barker and Langston (1987) from modeling teleseismic body waves.

2. Moment tensor

We used a time-domain iterative inversion method of Kukuchi and Kanamori (1991) that inverts teleseismic body waves to determine the mechanisms and rupture process. The rupture is represented as a sequence of subevents distributed in space and time. The subevent moment tensors are also allowed to vary. The number of unknowns is limited from observational constraints and a grid search is performed over the remaining free parameters including hypocenter depth, rupture direction, subevent rise time, and rupture velocity to find the best waveform fit.

The Green's functions were computed using the Haskell propagator matrix method (e.g., Haskell, 1962, Bouchon, 1976). We used a velocity model of Ichinose et al. (2004) that was calibrated using an iterative inversion method on regional seismograms (e.g., Nolet et al., 1986; Ichinose et al., 2003). The PS-9 velocity model of Langston and Blum (1977) was used as an initial model and includes the slower zone of subducting slab crust. The calibrated model has slower mid-crustal velocities and a steeper and faster velocity gradient in the upper crust (**Figure**

3). We account for teleseismic P-wave attenuation assuming an attenuation operator t^* of 1 sec (Langston and Helmberger, 1975). The attenuation operator $t^*=t/Q$ is integrated over the travel path where t is the travel time and Q is the quality factor.

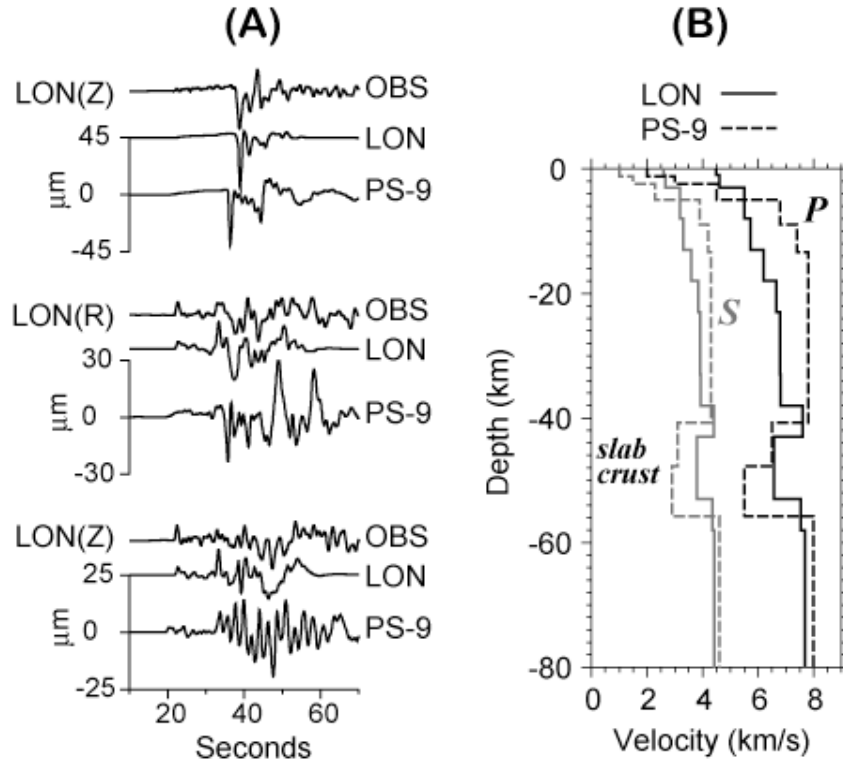


Figure 3. (A) Observed and predicted displacement seismograms for the 1999 Satsop, Washington Earthquake recorded at station LON. We used a calibrated LON model assuming the earthquake moment tensor to calculate synthetics up to 1 Hz and compared them to synthetics computed using the PS-9 model (Barker and Langston, 1987) to show that it improves the fit in amplitude and phase with the observed data. (B) P- and S-wave velocity profiles of the calibrated and PS-9 models.

Figure 4a shows a map of teleseismic stations that yielded teleseismic P-waveforms or first motion polarities for the 1949 earthquake. **Figure 4b** shows the fit between observed and predicted P-waveforms. We applied the instrument corrections to the Green's function to avoid instabilities due to the instrument deconvolution to digitized data. We assume 2 subevents with the second subevent occurring between 0 and 5 sec. The grid search results in an optimal rise time of 3 sec that best fits the frequency character of the waveform data. The resolution of the rupture velocity is poor therefore it was fixed at 3.5 km/s or 80% of the shear wave velocity at 60 km depth. **Table 1** lists the mechanisms and depths for the two subevents. The first subevent has a different mechanism than the second subevent at 4.6 sec, 6 km to the south at a direction of 170° (**Figure 5**). The sum of the 2 different mechanisms is a 0°N striking fault plane dipping 66°E and the total seismic moment (M_0) is 1.28×10^{26} dyne-cm (M_w 6.7). First motion polarities shown in **Figure 5A** from stations Berkeley (BRK), Bogotá (BOG), Pasadena (PAS), Saint Louis (SLM), and Weston (WES) best fits the dip of the high angle fault plane for the first subevent including BOG not used by Baker and Langston (1987). BOG is near nodal which may explain why SP and LP first motions were difficult to interpret.

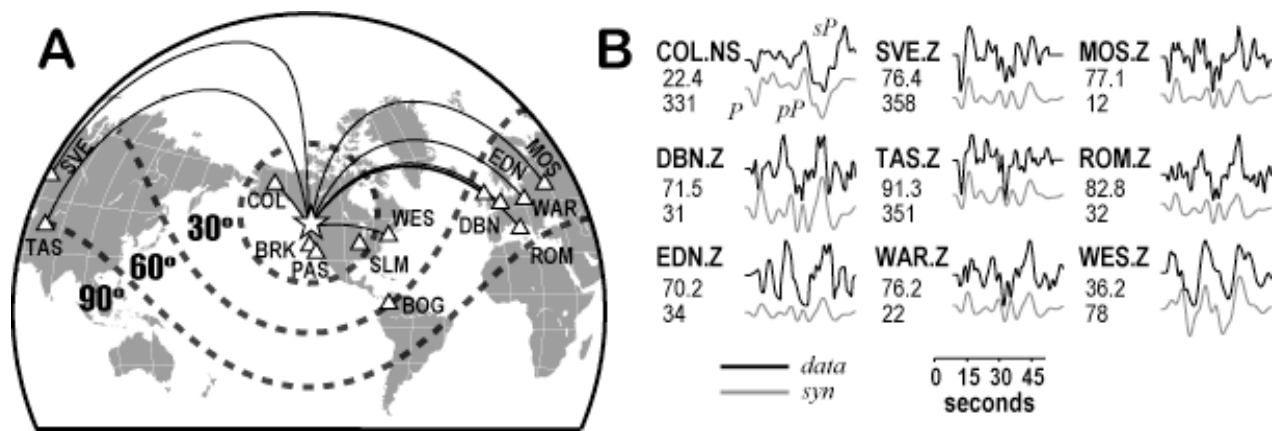


Figure 4. (A) Teleseismic stations that recorded the 1949 Olympia, Washington earthquake. (B) Observed and predicted teleseismic P-waves used in the moment tensor inversion. Epicenter distance in ($^{\circ}$) and source-receiver azimuth are listed below the station code.

Table 1. 1949 Olympia Earthquake Moment Tensor

Subevent	Nodal Plane 1 Strike/Dip/Rake	Nodal Plane 2 Strike/Dip/Rake	Depth (km)	M_0 (dyne-cm)	T_0 (s)
1	204/28/-83 $^{\circ}$	16/62/-93 $^{\circ}$	60	0.58×10^{26}	0
2	233/36/-31 $^{\circ}$	349/72/-122 $^{\circ}$	58	0.76×10^{26}	4.6
sum	223/31/-51 $^{\circ}$	0/66/-111 $^{\circ}$	-	1.28×10^{26}	-

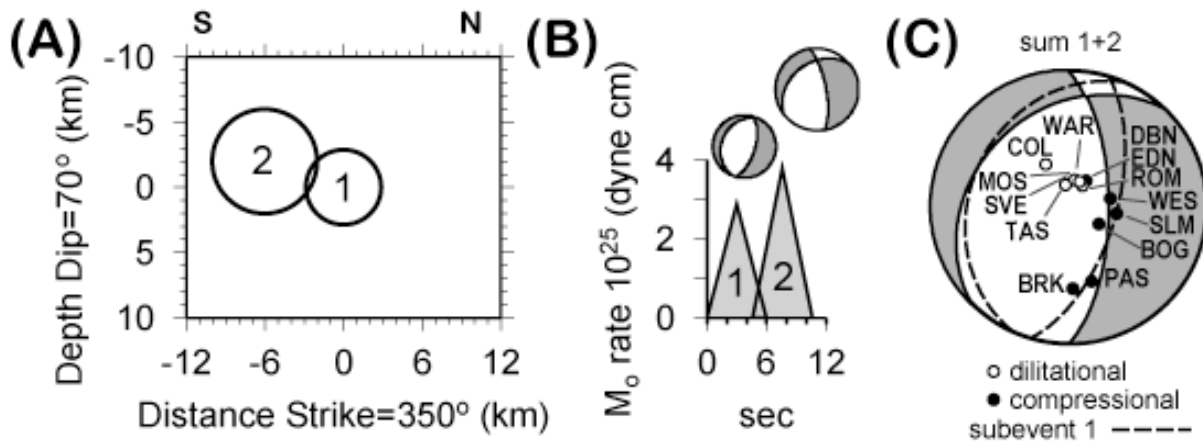


Figure 5. (A) The 1949 Olympia earthquake subevent locations. The origin is at a depth of 60 km. (B) Subevent moment tensors and moment rate source time function (Table 1). (C) The shaded mechanism shows the overall moment release while the nodal planes with dashed lines are from the first subevent.

The southward rupture propagation is difficult to confirm because PAS is the only available observation toward the south. PAS ($\Delta=13^{\circ}$) also has a P-wave path bottoming in the transition zone complicated by triplicated P-waves from the 410-km discontinuity. We compared the digitized PAS Benioff record from the 1949 earthquake with the digital broadband seismogram of the 2001 Nisqually earthquake. A Benioff 1-90 sec instrument response was convolved with the Nisqually record for a better comparison (Figure 6). The correlation of amplitudes and phases between the two observed P-wave vertical components and synthetics confirm that they both have similar seismic moments, mechanisms, and hypocenter depths. Forward modeling of

P-waveforms using f-k synthetics computed from the AK135 1-D layered global velocity model (Kennett et al., 1995) at different hypocenter depths (**Fig. 6**) indicate that the 1949 and 2001 earthquakes had hypocenter depths near 60 km, 10 km below the slab interface.

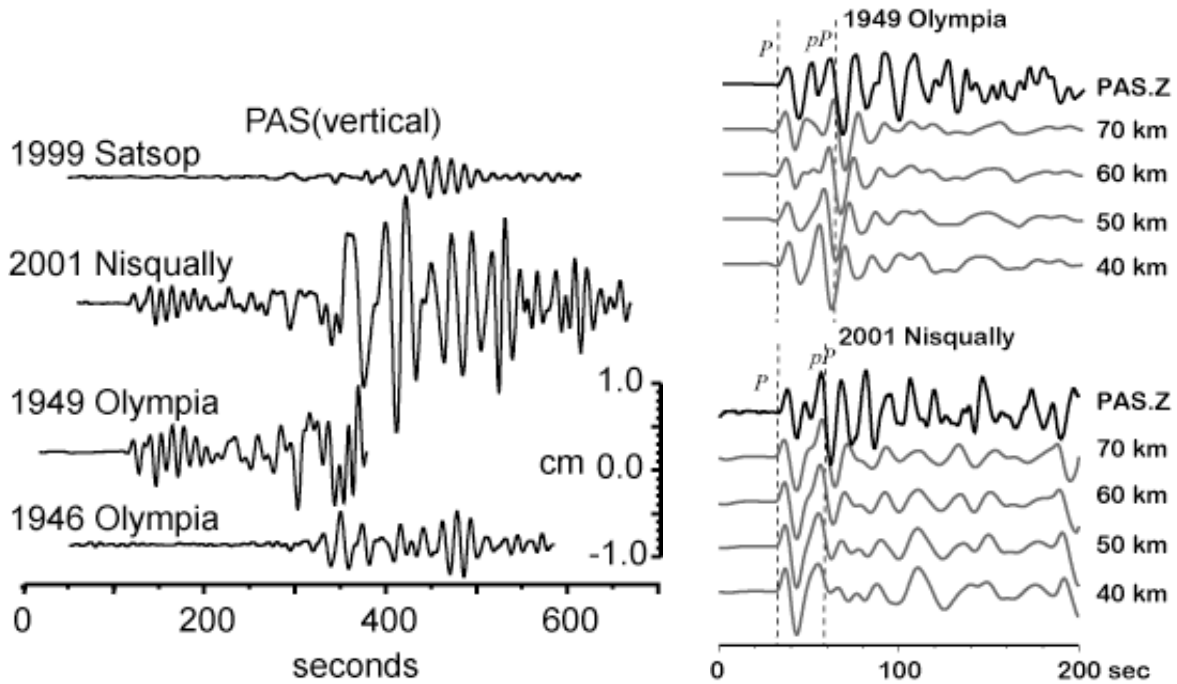


Figure 6. (right) Digitized seismograms from PAS ($\Delta=13^\circ$) of the historical 1946 and 1949 Olympia earthquakes compared to modern digital records of the 1999 Satsop (M_w 5.8) and 2001 Nisqually (M_w 6.8) earthquakes. The modern broadband records were instrument corrected to displacement and then filtered to a similar response of a 1-90 sec Benioff instrument. (left) Observed vertical component P-waves at PAS compared with synthetics computed assuming the estimated mechanisms for each earthquake at 10 km hypocenter depth increments.

3. Finite-Fault Rupture Model

We inverted teleseismic P-waves for the spatial and temporal distribution of slip and rake. Our method is explained by Thio et al. (2004) and is similar to the multiple time window method of Hartzell and Heaton (1983). The fault plane is described by a grid of points for which Green's functions are computed at each grid to observation point. A propagating slip band is imposed from the hypocenter and propagates at a fixed number of time steps. This slip band is characterized by maximum rupture velocity and rise time. Grid points that are contained within a slip band, at each time step, are combined and cast into a set of normal equations. The normal equation is solved simultaneously using a least squares solver with a positivity constraint to disallow reversed slip vectors (Lawson and Hanson, 1974). A smoothing condition is imposed where the amplitude of slip at one point is forced to be equal to its neighbors. Thio et al. (2004) allows for variable rake, in which case every initial rake vector is split into 2 conjugate vectors where the new rake is different from the initial by $\pm 45^\circ$. A strong rake smoothing constraint causes the 2 conjugate vectors to become equal yielding the orientation of the initial rake vector.

The fault is parameterized as a rectangular plane 36 km along strike and 33 km down dip. The fault plane is divided into a grid of 12 by 11 subfaults using a size of 3×3 km. The plane is oriented in a $N0^\circ E$ direction dipping $66^\circ E$ (**Fig. 5C**) assumed from the moment tensor inversion (**Table 1**). We do not include subfault dynamics because of the poor quality and quantity of

data. Computing a single Green's function for each subfault is adequate (*e.g.*, Beresnev and Atkinson, 2001). The USGS/NEIC hypocenter is located near the middle of the fault grid adjacent to the 2001 Nisqually earthquake hypocenter. We allow the rupture to evolve temporally based on a maximum rupture velocity of 3 km/s, a minimum rise time of 0.5 sec, and a maximum rise time of 1 sec. We expect rise times of about 0.8 to 1.1 sec (*e.g.*, Heaton, 1990; Somerville et al., 1999). Any point on the fault can slip either 1 or 2 times after the passage of the rupture front. The 14 time windows are spaced 0.5 sec apart. The slip at each grid point is summed using an isosceles triangle shaped source-time function with 0.5 s rise and 0.5 s fall-off. We inverted teleseismic P-waves and depth phases from 9 stations (**Figure 7**) for the kinematic rupture model using the multiple time window methodology. The rupture model (**Figure 8**) has a total M_0 of 1.9×10^{26} dyne-cm (M_w 6.8) and its asperity locations are within 2-3 km of the simple rupture model shown in **Figure 5** both indicating a southward rupture direction of about 3 to 6 km from the hypocenter.

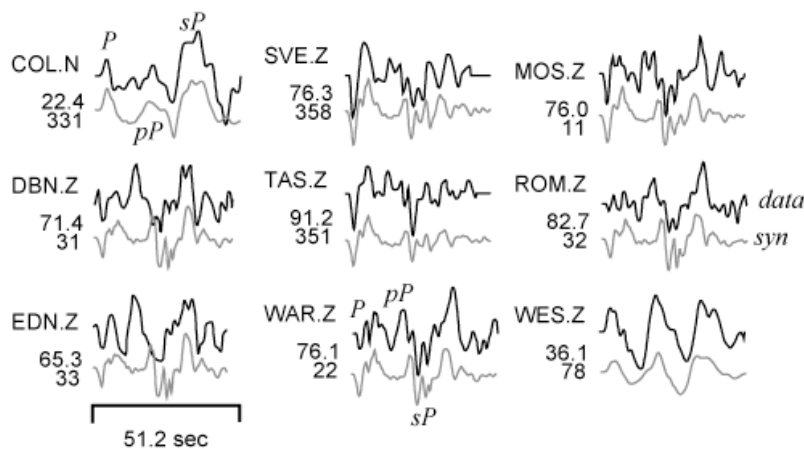


Figure 7. Observed and predicted teleseismic P-waves and depth phases computed from the kinematic slip model shown in the following figure. Epicenter distance in ($^{\circ}$) and source-receiver azimuth are listed below the station code.

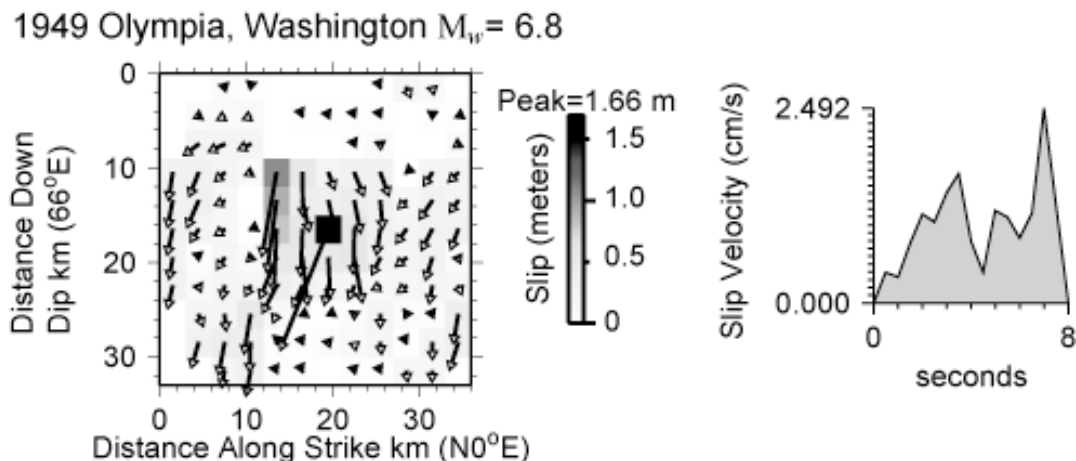


Figure 8. The 1949 Olympia earthquake cumulative slip and rake distribution from the kinematic rupture model estimated using the multiple-time window inversion. The rake vectors point in the direction of the hanging wall motion. The hypocenter is at 60 km depth and is located at 16 km down dip and 20 km along strike.

4. Intraslab Source Scaling Relations

The rupture models of intraslab earthquakes have important implications for earthquake source scaling relations used for the simulation of strong-ground motions (e.g., Somerville et al., 1999). The relation between seismic moment and fault rupture area is particularly important because it defines the static stress drop, which affects the rate of energy release of the earthquake. It is commonly thought that deeper intraslab earthquakes have smaller rupture areas and hence larger static stress drops and potentially stronger ground motions than crustal or subduction zone interplate earthquakes of the same magnitude.

Table 2. Cascadia Intraslab Earthquake Source parameters

	1949 Olympia	1965 Seattle-Tacoma	2001 Nisqually
M_o (dyne-cm)	1.91×10^{26}	9.43×10^{25}	1.66×10^{26}
Rupture Area	396 km ²	248 km ²	496 km ²
Average Slip	0.43 m	0.52 m	0.43 m
Combined Area of Asperities	36 km ²	28 km ²	45 km ²
Average Asperity Slip	1.12 m	2.15 m	1.67 m

Figure 9 compares the combined area of asperities (A_a) and seismic moment from the 1949 earthquake (**Table 2**) with those obtained using similar procedures and methods for 2 other Puget Sound earthquakes (Ichinose et al., 2004). We included measurements from several Japanese (Asano et al., 2003; Morikawa and Sasatani, 2004) and Mexico intraslab earthquakes (Hernandez et al., 2001; Iglesias et al., 2002; Yamamoto et al., 2002; García et al., 2004). These are compared with A_a values from global crustal earthquakes (Somerville et al., 1999). To estimate A_a , we first identify the subfaults with slip contrast greater 1.5 times the average slip (**Table 2**). These are then summed and multiplied by the subfault area to calculate the combined area of asperities. The data in **Figure 9** show a linear correlation between logarithm of A_a and M_o with a correlation coefficient of 0.6 for intraslab and 0.8 for strike-slip earthquakes both with statistically high significance levels.

We estimated a relation between A_a as a function of M_o for intraslab earthquakes using linear regression. As a reference, the relation from Somerville et al. [1999] for global crustal earthquakes is,

$$\log_{10}(A_a) = 0.67 M_o - 15.3 \quad (\text{Eq. 1})$$

assuming self-similarity (constrained slope=2/3), and

$$\log_{10}(A_a) = 0.87 M_o - 20.2 \quad (\text{Eq. 2})$$

for unconstrained slope. The best fit to intraslab earthquakes is,

$$\log_{10}(A_a) = 0.57(\pm 0.06) M_o - 13.5(\pm 1.5) \quad (\text{Eq. 3})$$

with the average residual of 0.9 with a standard deviation of 16.1. A relation including both types of the data gives average residual of 28.3 with a standard deviation of 254.7. We excluded data from Mexico estimated from S-wave spectra because they probably reflect the area of the largest asperity rather than combined area. Nevertheless, the rupture area or A_a for all intraslab earthquakes plot below the relation estimated using the global strike-slip and intraslab

earthquakes together (**Figure 8**). The relationship for only intraslab earthquakes removes the large bias in residuals and significantly lowers the standard deviation in residuals.

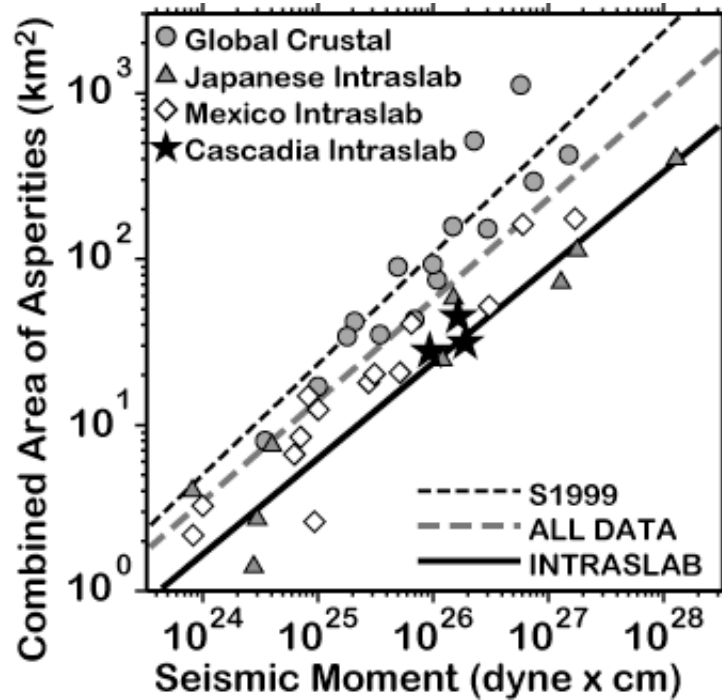


Figure 9. The combined area of asperities versus seismic moment for global crustal and intraslab earthquakes. S1999 is the relation from *Somerville et al.* [1999] assuming self-similarity for global crustal earthquakes.

5. Conclusions

We infer that the A_a for deeper intraslab earthquakes have a significantly smaller combined area of asperities than those from shallower strike-slip earthquakes with the same M_0 . This relative difference leads to a 3-fold increase in stress drop at 10^{24} dyne-cm increasing to a 5-fold increase at 10^{28} dyne-cm. This apparent increase in stress drop can explain the stronger ground motions observed for intraslab earthquakes relative to ground motion attenuation models for subduction zone interplate earthquakes at the same magnitudes (e.g., Atkinson and Boore, 2001).

We conclude that the largest Puget Sound intraslab earthquakes between 1949 and 2004 have normal-faulting mechanisms with down dip trending T-axis and they also have similar source scaling characteristics as those observed in Japan and Mexico. In addition, the rupture process appears to be best characterized as a mode 3 type crack common to most large dip-slip earthquakes as the 3 largest intraslab earthquakes in the Puget Sound (1949 Olympia, 1965 Seattle Tacoma, and 2001 Nisqually earthquakes) all ruptured with slip distribution elongated along strike direction (e.g., Ichinose et al., 2004).

Acknowledgements. We thank Paul Roberts and Don Helmberger for access to the Kresge Laboratory and Caltech filmchip archives. This research was funded by USGS-NEHRP grant award 04HQGR0050.

References

Asano, K., T. Iwata, and K. Irikura (2003), Source characteristics of shallow intraslab earthquakes derived from strong motion simulations, *Earth Planets Space*, 55, e5-e8.

- Atkinson, G. M., and D. M. Boore (2003), Empirical ground-motion relations for subduction zone earthquakes and their application to Cascadia and other regions, *Bull. Seismol. Soc. Am.*, 93(4), 1703-1729.
- Baker, G. E., and C. A. Langston (1987), Source parameters of the 1949 magnitude 7.1 south Puget Sound, Washington, earthquake as determined from long-period body waves and strong motions, *Bull. Seismol. Soc. Am.*, 77, 1530-1557.
- Beresnev, I., and G. Atkinson (2001), Subevent structure of large earthquakes-A ground motion perspective, *Geophys. Res. Lett.*, 28, 53-56.
- Bouchon, M. (1976), Teleseismic body wave radiation from a seismic source in a layered medium, *Geophys. J. R. Astr. Soc.*, 47, 515-530.
- Dobson, D. P., P. G. Meredith, S. A. Boon (2002), Simulation of subduction zone seismicity by dehydration of serpentine, *Science*, 298, 1407-1410.
- Garcia, D., S. K. Singh, M. Herraiz, J. F. Pacheco, M. Ordaz (2004), Inslab earthquakes of central Mexico: Q, source spectra, and stress drop, *Bull. Seismol. Soc. Am.*, 94(3), 789-802.
- Haskell (1962), N. A., Crustal reflection of plane P and SV-waves, *J. Geophys. Res.*, 67, 4751-4767.
- Hartzell, S. H., and T. H. Heaton (1983), Inversion of strong motion and teleseismic waveform data for the fault rupture history of the 1979 Imperial Valley, California earthquake, *Bull. Seism. Soc. Am.*, 73, 1553-1583.
- Hernandez, B, N. M. Shapiro, S. K. Singh, J. F. Pacheco, F. Cotton, M. Campillo, A. Iglesias, V. Cruz, J. M. Comez, and L. Alcantara (2001), Rupture history of September 30, 1999 intraplate earthquake of Oaxaca, Mexico (Mw=7.5) from Inversion of strong-motion data, *Geophys. Res. Lett.*, 28(2), 363-366.
- Ichinose, G. A., Hong Kie Thio, and P. G. Somerville (2003), Rupture process of the 1944 Tonankai earthquake (Ms 8.1) from the inversion of teleseismic and regional seismograms, *J. Geophys. Res.*, 108(B10), 2497, doi: 10.1029/2003JB002393.
- Ichinose, G. A., H. K. Thio, P. G. Somerville (2004), Rupture process and near source shaking of the 1965 Seattle-Tacoma and 2001 Nisqually intraslab earthquakes, *Geophys. Res. Lett.*, 31, L10604, doi: 10.1029/GL019668.
- Iglesias, A., S. K. Singh, J. F. Pacheco, and M. Ordaz (2002), A source and wave propagation study of the Copalillo, Mexico, earthquake of 21 July 2000 (Mw 5.9): Implications for seismic hazard in Mexico City from inslab earthquakes, *Bull. Seismol. Soc. Am.*, 92(3), 1060-1071.
- Kennett, B., L., N., E. R. Engdahl, and R. Buland (1995), Constraints on seismic velocities in the Earth from traveltimes, *Geophys. J. Int.*, 122, 108-124.
- Kikuchi, M., and H. Kanamori (1991), Inversion of complex body waves-III, *Bull. Seism. Soc. Am.*, 81, 2335-2350.
- Langston, C. A., and D. E. Blum (1977), The April 29, 1965, Puget Sound earthquake and the crustal and upper mantle structure of western Washington, *Bull. Seism. Soc. Am.*, 67, 693-711.
- Langston, C. A., and D. V. Helmberger (1975), A procedure for modeling shallow dislocation sources, *Geophys. J. R. Astr. Soc.*, 42, 117-130.
- Lawson, C. L., and R. J. Hanson (1974), *Solving Least Squares Problems*, Englewood Cliffs, NJ: Prentice-Hall.
- Morikawa, N., and T. Sasatani (2004), Source models of two large intraslab earthquakes from broadband strong ground motions, *Bull. Seismol. Soc. Am.*, 94(3), 803-817.
- Nolet, G., J. van Trier, and R. Huisman (1986), A formalism for nonlinear inversion of seismic surface waves, *Geophys. Res. Lett.*, 13, 26-29.
- Nuttli, O. W. (1952), The western Washington earthquake of April 13, 1949, *Bull. Seismol. Soc. Am.*, 42, 21-28.

- Somerville, P., K. Irikura, R. Graves, S. Sawada, D. Wald, N. Abrahamson, Y. Iwasaki, T. Kagawa, N. Smith, and A. Kowada (1999), Characterizing crustal earthquake slip models for the prediction of strong ground motion, *Seismol. Res. Lett.*, 70, 59-80.
- Thio, H. K., R. W. Graves, P. G. Somerville, T. Sato, and T. Ishii (2004), A multiple time window rupture model for the 1999 Chi-Chi earthquake from a combined inversion of teleseismic, surface wave, strong motion, and GPS data, *J. Geophys. Res.*, 109, B08309, doi:10.1029/2002JB002381.
- Wiest, K., D. I. Doser, and J. Zollweg (2003), Source processes of Western Washington intraslab earthquakes (1939-1965), (abstract), *Seismol. Res. Lett.*, 74, 239.
- Yamamoto, J., L. Quintanar, C. J. Rebolgar, and Z. Jimenez (2002), Source characteristics and propagation effects of the Puebla, Mexico, earthquake of 15 June 1999, *Bull. Seismol. Soc. Am.*, 92(6), 2126-2138.

Nontechnical Summary

Intraslab earthquakes occur deep within the Cascadia subduction zone deep (> 40 km) beneath the Puget Sound of western Washington. These types of earthquakes have occurred frequently including in 1949 Olympia (M_w 6.8), 1965 Seattle-Tacoma (M_w 6.8), 1999 Satsop (M_w 5.9) and 2001 Nisqually (M_w 6.8). Because of this frequent occurrence, the hazards they pose are nearly equal to those from other seismic sources in the region for time scales relevant to retrofitting ports, buildings, lifelines, and bridges. The recent 2001 Nisqually earthquake caused over a billion dollars in losses. While retrofitting limited damages, continued efforts are needed because an earthquake closer to the major population centers of Seattle or larger in magnitude will cause more damage and disruption. The reexamination of historical earthquake seismograms using modern methods along with the analysis of modern digital seismograms from recent earthquakes improves strong motion prediction more than random scenarios. For example, the reanalysis of the 1949 Olympia, Washington earthquake in this study yielded a faulting mechanism that contrasts greatly from previous studies. The new rupture models from this study can be used in future assessments for ground motion simulation. In addition, we identify a different earthquake source scaling relation indicating that intraslab earthquakes in Cascadia and in other global subduction zones release more energy over a smaller area than typical crustal earthquakes in southern California. This may explain the higher recorded peak ground accelerations than those recorded from other earthquakes with the same size.